CAAP Quarterly Report

[01/02/2024]

Project Name: "All-in-One Multifunctional Cured-In-Place Structural Liner for Rehabilitating of Aging Cast Iron Pipelines"

Contract Number: 693JK32250009CAAP

Prime University: North Dakota State University

Prepared By: [Ying Huang, ying.huang@ndsu.edu, 701-231-7651]

Reporting Period: [09/28/2023 – 12/27/2023]

Project Activities for Reporting Period:

In the 4th quarterly report, Tasks 2.1, 2.2, 3.1, 3.2, 3.3, 3.4, 4.1, 4.2, and 5.1 were carried out as proposed. In this quarter (Quarter 5), the research team has consistent progress on selected tasks. The summaries of the key activities completed during the fifth reporting period are provided below.

Task 2.1 Preparation of Vitrimer Epoxy Resins, characterization, and optimization of the processing and curing conditions (60%): In this reporting period, the research team (Dr. Long Jiang and Austin Knight, Ph. D. student from NDSU) performed new modified formations of self-healing polymer to overcome tensile properties reduction issue due to the increased UV-curing duration. The findings are summarized below:

(1) Synthesis and Curing Characteristics: The non-functional catalyst (NFC) used in the last quarter was successful in preventing the gelling of the resin and the synthesis time increased from 20 minutes to 5 hours to ensure the complete conversion. However, the longer synthesis time led to a decrease in the tensile properties, due to the sharp increase in viscosity with higher conversions inhibiting polymerization during the UV-curing. A reactive diluent to prevent the high viscosity induced polymerization inhibition was added. Therefore, formulations of the synthesized resin and MRD with ratios 1:0, 1:0.5, 1:1, 1:3, and 0:1 were prepared, and the tensile properties were tested.

Task 2.2 Investigating self-healing and mechanical properties of vitrimer epoxy resins (55%): The research team (Dr. L. Jiang, Dr. Y. Huang, and Austin Knight, Ph. D. student from NDSU) investigated the self-healing and mechanical performances of the self-healing polymer in subtask 2.1, the tensile and self-healing properties were evaluated, and the results are presented below:

(1) Tensile Properties of Self-Healing UV-curable Adhesive with Reactive Diluent: Further tensile testing was done with varying amounts of methacrylate reactive diluent (MRD) to determine the concentration that led to the most desirable properties. As shown in Figure 1, the 1:1 formulation showed the best tensile properties, workability, and dimensional stability.

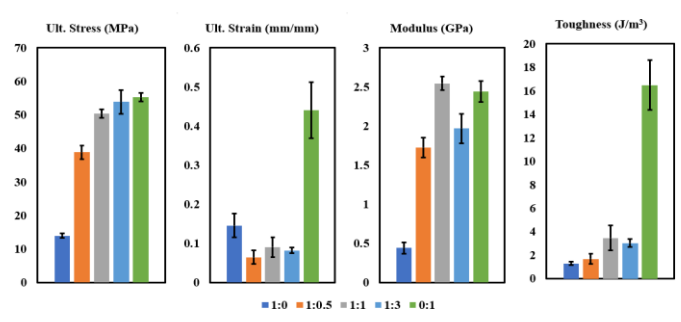

Figure 1. A summary of the tensile properties of synthesized formulations with various resin and reactive diluent ratio. The properties of the synthesized resin increased with increasing reactive diluent content, however, the 1:3 and 0:1 formulation had extreme warpage and shrinkage respectively.

(2) Self-Healing of UV-Curable Adhesive Coatings: Formulations were applied to steel substrates and cut through the entire thickness of the coating. The cut profile and depth were measured before and after healing by heating the coatings using a hot press for 10 minutes at 120°C and 50 lbs. The repair ratio of each formulation was calculated by measuring the depth of the cut before and after healing (Figure 2). The 1:1 formulation remains the best formulation as the 1:3 formulation has warping issues when UV-curing.

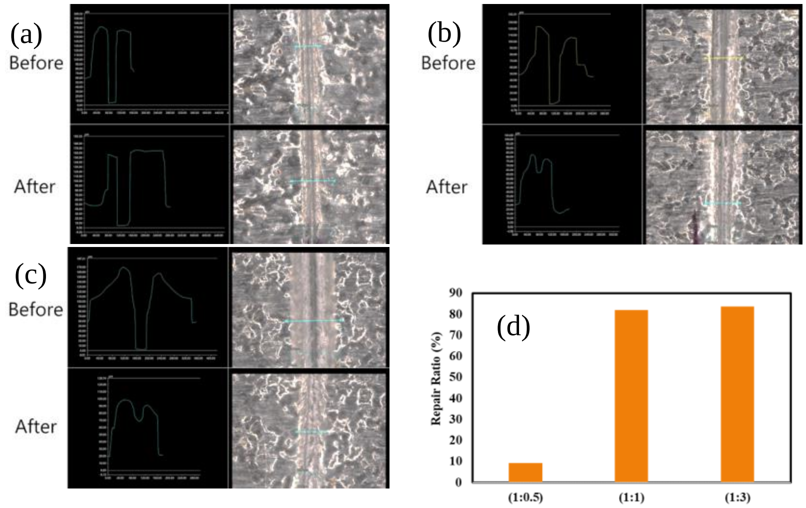

Figure 2. Profile images of before and after healing the (a) 1:0.5, (b) 1:1, and (c) 1:3 formulation. (d) Repair ratios of the self-healing coatings. As expected, the formulation with a greater amount of reactive diluent showed better self-healing performance.

Note: The 1:0 and 0:1 formulation could not be cured into thin films on the substrate, as the 1:0 formulation was too viscous and the 0:1 formulation was not viscous enough and spread too thin to cure. Therefore, only the 1:0.5, 1:1, and 1:3 formulations were investigated.

Task 3.1 High Mechanical Performance (60%): During this reporting period, the research team (Dr. Ying Huang, Dr. Zhibin Lin, Dr. Xingyu Wang, Muhammad Imran Khan, Master student from NDSU, Tofatun Jannat and Zahoor Hussain, Ph. D. students from NDSU) conducted experimental studies on nanoparticle reinforcement by developing a new nanoparticles dispersion method. The key findings are provided below:

(1) Nanoparticle Dispersion Method Based on Carboxymethyl Cellulose (CMC) Functionalization: A new functionalization technique using carboxymethyl cellulose (CMC) for nanofiller dispersion was developed, eliminating the need for ultrasonication and high-speed dispersion, thus reducing energy costs and shortening dispersion time. All three nanofillers were functionalized using identical surface treatment procedures. The weight concentrations of CMC and nanofillers were identical to the samples prepared by the previous dispersion method (0.5% 1.0%, 1.5%, and 2.0%). Surface characterization of CMC modified nanoparticles and mechanical properties of nanocomposite were evaluated and the results are presented in Figure 3.

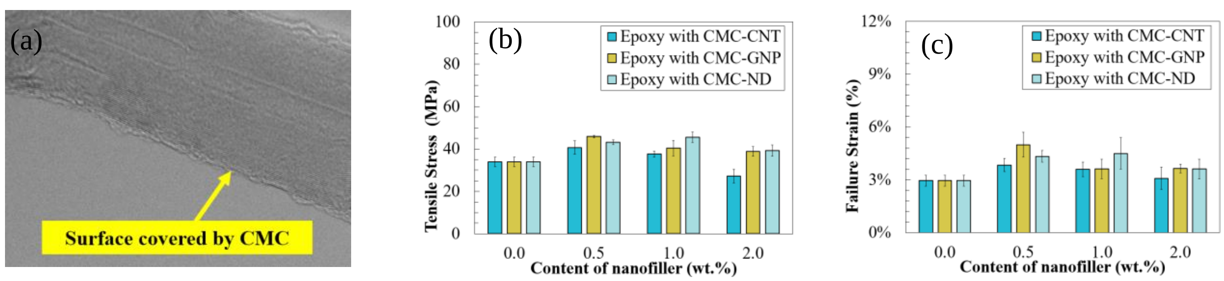

Figure 3. (a) TEM image of CMC modified CNT. (b) Tensile strength and (c) failure strain of samples reinforced by CMC modified CNT, GNP, and ND.

Task 3.3. Reducing the Permeability and Investigating the Interfacial Bonding Chemical Analysis (40%): By following the previous reporting period, the research team (Dr. Liangliang Huang, Qiuhao Chang, Ph. D. student from University of Oklahoma) focused mainly on developing computational models to simulate hydrogen diffusions properties on nanoparticle surface:

(1) Nanopore Surface Comparisons: When investigating hydrogen storage, one must consider the possibility of hydrogen loss by leakage through nanopores or by hydrogen adsorption and reactions at surfaces. Figure 4 illustrates hydrogen density profiles and self-diffusion coefficients in kaolinite pores with inward-facing surfaces of $AlO_4(OH)_2$ and SiO_4. The results in Figure 4 display insignificant changes in hydrogen properties from one kaolinite surface to the other. Consequently, it is concluded that the kaolinite surface compositions do not influence H_2 transport due to weak interactions with both surfaces in general. Therefore, for this work, further results for H_2 in kaolinite pores will only be presented from simulations utilizing inward-facing $AlO_4(OH)_2$ surfaces.

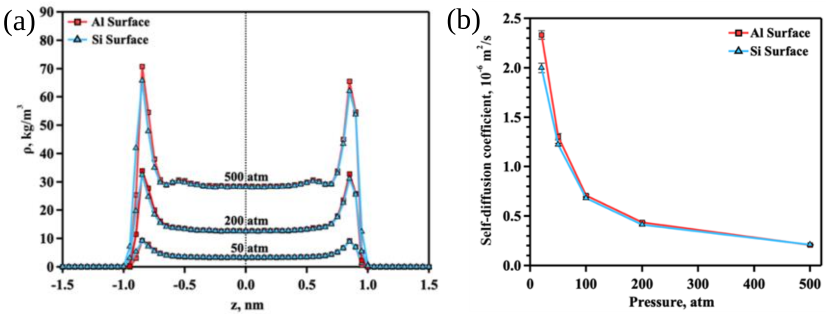

Figure 4. H_2 in 2 nm kaolinite pores with inward-facing surfaces of $AlO_4(OH)_2$ and SiO_4. (a) Density profiles along the z-direction (lower pore surface to upper pore surface) and (b) total self-diffusion coefficients.

(2) Interaction of Hydrogen in Kaolinite and Graphene Nanopores: Figure 5a shows negative values for interaction energies between hydrogen and both pore types, indicating an affinity of H_2 molecules for the wall surfaces. However, the results reveal that attractive intermolecular interactions between H_2 molecules and graphene are more than double those between H_2 molecules and kaolinite. H_2 molecules lining the graphene pore surfaces at a density ~35% higher than the kaolinite pore surfaces at pressures of 100 and 500 atm, indicating H_2 clearly prefers interacting with graphene. Strong attraction to and adsorption of gas molecules at pore surfaces can also be evidenced by increasing trends in self-diffusion coefficients with increasing pressure.

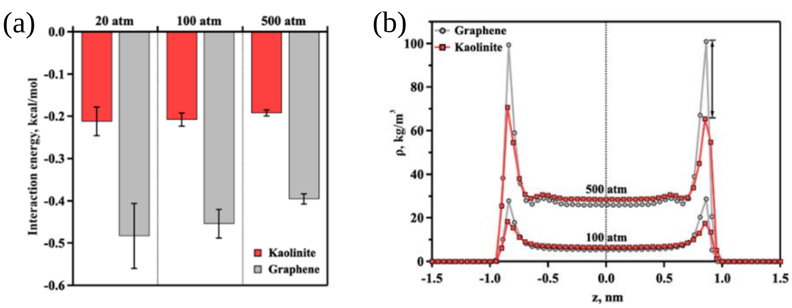

Figure 5. Interaction of H_2 in 2 nm kaolinite (Al surface) and graphene pores. (a) Normalized gas-solid interaction energies, and (b) z-direction density profiles under 20-500 atm.

Task 3.4 Finite Element Numerical Analysis to Guide the Design of the Developed high-performance healable CIPP Structural Liner (40%): During this reporting period, the research team (Dr. Chengcheng Tao, Junyi Duan, Ph.D. student from Purdue University) have conducted finite element analysis (FEA) for pipelines rehabilitated by CIPP liners as summarized below:

(1) The adhesive layer in-between pipe and cure-in-place liner has always been rarely studied and the epoxy resin is the most widely adopted in the applications. Additionally, the pipe elbow is also a concern, which is a curved pipe, typically 90 degrees, changing the direction of pipeline transportation. Therefore, in this study, finite element analysis (FEA) was utilized to examine the mechanical responses of straight and curved CIPP liner system with epoxy adhesive layer.

(2) Effect of Thickness of Adhesive Layer in Straight and Curved Pipe: FEA analysis was performed for straight and curved pipe applied with CIPP liner systems, with three adhesive layer thicknesses (0, 0.5, and 1 mm). The dimensions of CIPP liner system are outlined in Figure 6(a). The model simulates the underground CIPP liner system that works under a high-pressure condition of 1.5 MPa. Results presented in **Error! Reference source not found.** indicates that, adhesive layer exerts negligible influence on the CIPP liner system; however, the maximum stress at pipe elbow increases 18% compared to the straight pipe.

(a)	Straight pipe	Curved pipe	Liner
Length (mm)	1200	2400	Same as pipe
Thickness (mm)	15	15	3
Inner radius (R - mm)	300	300	Controlled by varied adhesive layer thickness (0, 0.25 and 1 mm)

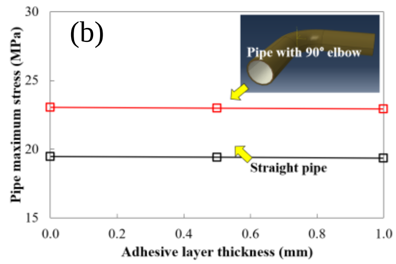

Figure 6. (a) The dimensions of the CIPP liner system. (b) The pipe maximum stress versus the thickness of adhesive layer.

(3) The Effect of Corrosion Hole Size on the Straight CIPP Liner System: Three radii (r) of circular corrosion holes are considered including 25 mm, 50 mm, and 100 mm. The mechanical performance of CIPP liner system with respect of adhesive layer exhibits in Figure . In the presence of the adhesive layer, the maximum stress on the liner experiences a significant reduction for all three cases. However, the reduction in maximum stress on the pipe is only identified when the hole size is small (25 mm) but stabilizing as the hole size exceeds 50 mm. This phenomenon indicates liner can withstand in-pipe pressure when the hole is small, and pipe provides ultimate structural integrity of system when the hole surpasses a size compensable by the liner.

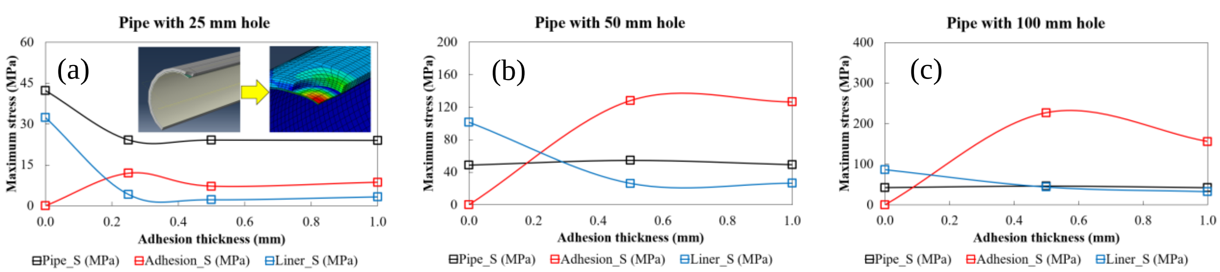

Figure 7. The mechanical performance of CIPP liner system with respect of adhesive layer.

(4) The Effect of Bonding Conditions Between Adhesive Layer to Pipe Wall: The bonding state is simulated using the friction coefficient in finite element analysis (FEA), with four factors ranging from 0 to 1, representing conditions from debonding to complete adhesion. The results are presented in Figure . As the size of corrosion hole in a pipe increases, the bonding condition between the pipe and adhesive layer becomes more significant in the pipe's maximum stress. For smaller holes, the impact of bonding on pipe performance is relatively minor. Furthermore, a thicker adhesive layer tends to reduce the maximum stress on the pipe, a trend that is more noticeable with smaller holes, as shown in Figure 8 (c) and (d).

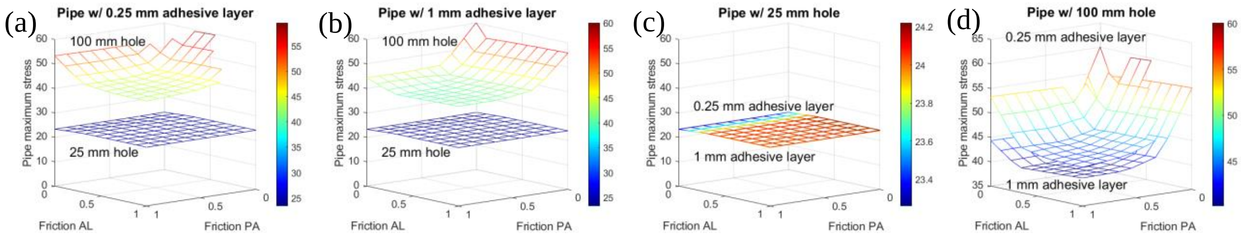

Figure 8. The effect of bonding condition between interfacial layers on pipe maximum stress.

Task 4.1 Development of Embedded Distributed Fiber Optic Sensors for Self-sensing Structural Liner (30%), and **Task 4.2** Investigating the load transfer between layers of the CIPP liner and the cast-iron substrate (30%): During this reporting period, the research team (Dr. Ying Huang and Dr. Xingyu Wang) conducted an experimental study on corporation distributed fiber optic sensors to CIPP liner system and investigated the load transfer between CIPP liner and steel substrate, the findings are presented below:

(1) Compatibility of the Smart Sensor-Liner System: To evaluate the compatibility between the sensor and liner, distributed optic fiber sensors were integrated into a commercial liner. The optic fiber sensors demonstrated strong adherence to the liner, as evidenced in Figure 9 (a), where the sensors remained firmly attached to the liner even under significant deformation. After that, the liner equipped with sensors was applied to a steel substrate using epoxy adhesive (Figure 9 (b)).

(2) Mechanical Deformation Detection and Shape Reconstruction via Sensor-Liner System: The smart sensor-liner system, integrated with fiber optic sensors, is designed to detect, visualize and quantify mechanical deformations. A sample with this system was subjected to buckling load, and strain data was captured by sensors arranged in 14 lines, each 1 cm apart. The obtained data was used in a polynomial fitting mathematical model, helped visualize the deformation. Increasing the polynomial fitting surface's order (both in X and Y dimensions) effectively represented the spatial distribution and magnitude of the strain on the buckled plate. The model's accuracy in depicting strain distribution was enhanced by adjusting the polynomial fitting orders, as detailed in Figure 10(f).

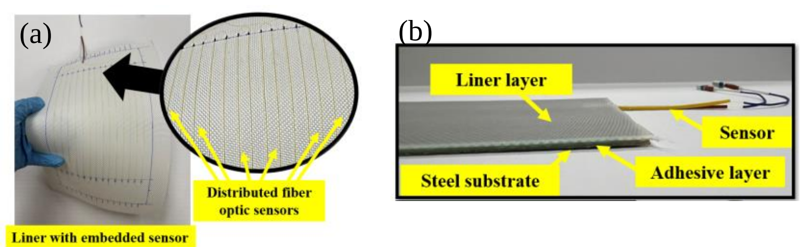

Figure 9. (a) Smart sensor-liner system, (b) sensor-liner system applied to flat substrate. For experimental simplicity, a 6 x 12” steel panel was utilized to examine the sensor-liner system.

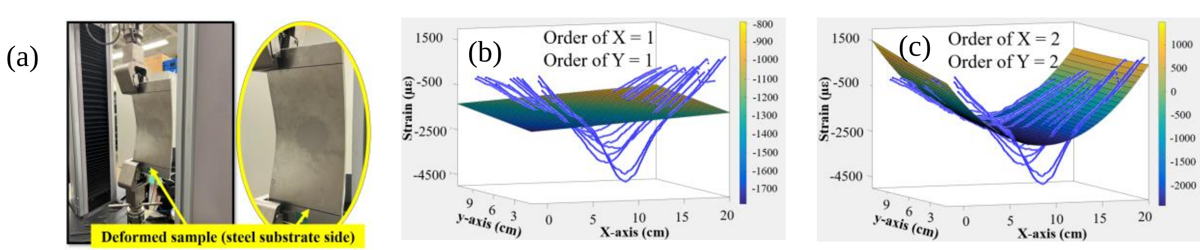

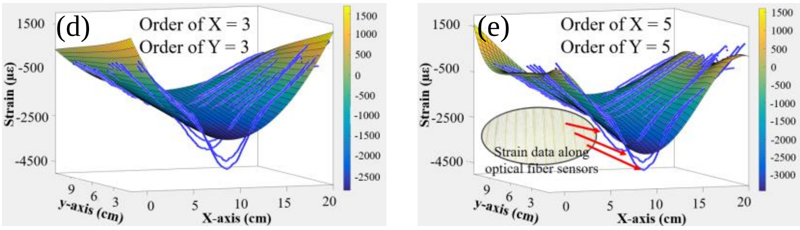

(f) R-square of the polynomial ftting

x \ y	1	2	3	4	5
1	3.9%	3.7%	3.6%	4.2%	4.4%
2	96.6%	99.0%	99.0%	99.5%	99.2%
3	99.5%	99.0%	99.4%	99.4%	99.2%
4	99.6%	99.6%	99.6%	99.6%	99.5%
5	93.4%	93.6%	99.6%	99.5%	99.5%

Figure 10. (a) A sample equipped with smart sensor-liner system undergoing buckling deformation. (b) to (e) Utilization of polynomial fitting to reconstruct the deformation, based on data from the smart sensor-liner system. (f) Sensitivity analysis of the polynomial fitting process.

Task 5.1 Development of CIPP liner risk index for the pipeline integrity management enhanced by AI algorithms (30%): During this period, the research team (Dr. Chengcheng Tao, Yizhou Lin, Ph.D. student from Purdue University) have conducted multi-scale simulation for pipeline integrity management, this report focuses on simulating the influence of fiber parameters on the strength of the fiber-reinforced adhesive layer. The Representative Volume Element (RVE) analysis and FEA were employed to investigate the various parameter effects on fiber composite, including fiber orientation (0° to 90°) and fiber volume friction (fvf) (0.5% to 9.5%). The findings are presented below:

(1) Effect of Fiber Orientation: The fiber orientation analysis revealed that the orientation of fibers relative to the loading direction significantly influences composite strength. The FEA in Figure 11 showed anisotropic and isotropic strength differences across orientations ranging from 0° to 90°. The maximum strength was observed when fibers were aligned parallel to the loading direction. A significant drop in strength occurred at approximately 18 degrees in anisotropic material. Isotropic material demonstrates a consistent even strength distribution across different orientations.
(2) Effect of Fiber Volume Fraction (fvf): fvf, a crucial factor in fiber composites, was adjusted by varying the fiber radius while keeping the number of fibers constant. Results shown in Figure 11(d) and (e) offer a detailed analysis of the relationship between composite strength and fvf.

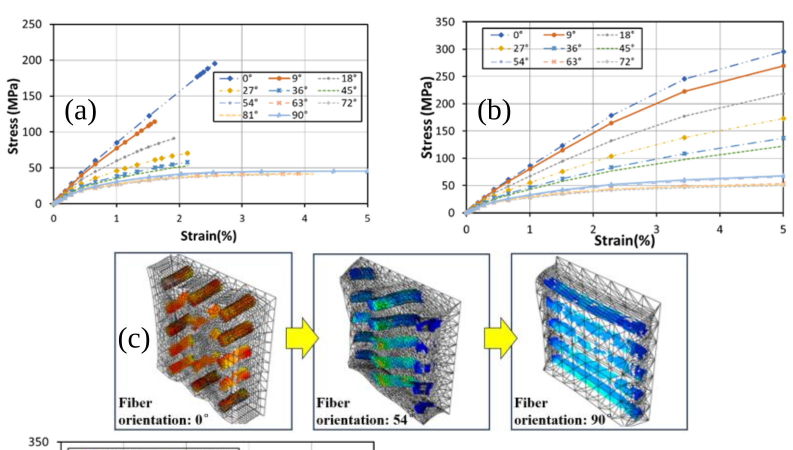

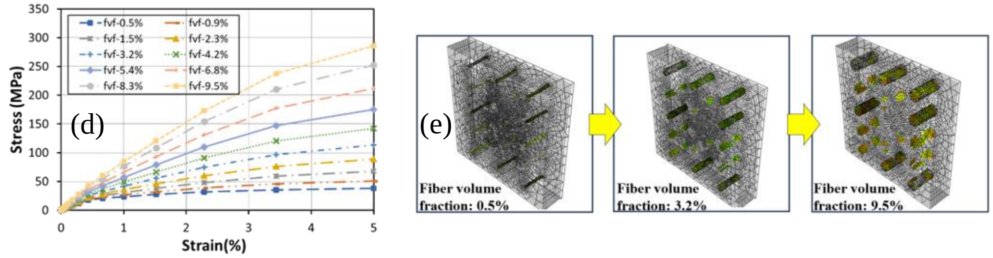

Figure 11. Stress-strain curve of fiber composite with fiber orientation viable. (a) in anisotropic material; (b) in isotropic material; (c) FEA model visualization; (d) Stress-strain curve of fiber composite single parameter study with fiber volume fraction variable, and (e) FEA model visualization.

Project Financial Activities Incurred during the Reporting Period:

The cost breakdown during the reporting period in each category according to the budget proposal is shown in Table 1. The actual spending may be slightly different.

Table 1. Cost breakdown

Category	Amount spent during Q5
Personnel	
Faculty and Postdoc	$3,060
Students (RA and UR)	$6,523.42
Benefits	$2,123.34
Operating Expenses	
Travel	$893.09
Materials and Supplies	$4,641.7
Recharge Center Fee	$938.5
Consultant Fee	$1,500
Subcontracts	$325.38
Indirect Costs	$8,856
Total	$28,536.05

Project Activities with Cost Share Partners:

The Match fund from NDSU for this project is coming from the tuition of the associated graduate students during their work on this project. During the reporting period (Q2), Zahoor Hussain (100%), Muhammad Imran Khan (100%), Austin Knight (35%), and Tofatun Jannet (46.15%) were hired on the project. The tuition for the four students during Q2 was estimated to be $14,562 at a rate of $463.73 per credit. The cost share from Purdue University include faculty salary $587.62, graduate student assistantship $6,315.89, benefits $1,720, and indirect cost of $178.96, which was amounted to be $12,295.63.

Project Activities with External Partners:

During this reporting period, George Ragula, our industry consultant, attended all the bi-weekly meetings with the research team. The research team attended the PHMSA R&D forum, hosted a booth, and met with many industries who are interested in the development of this project.

Potential Project Risks:

No potential risks were noticed during this reporting period.

Future Project Work:

The research team will continue working on Tasks 2.1, 2.2, 3.1, 3.2, 3.3, 3.4, 4.1, 4.2 and 5.1.

Potential Impacts on Pipeline Safety:

The newly developed self-healing epoxy exhibits excellent workability, self-healing capabilities, and mechanical properties, highlighting its potential to improve the safety of pipelines equipped with CIPP liners. Additionally, the novel nanoparticle dispersion method significantly enhances the mechanical properties of polymeric composites. The smart sensor-liner system demonstrates that distributed optical sensors are effective in detecting, visualizing, and quantifying mechanical deformations across the entire liner system. Analytical insights from the studies on the liner system modelling and fiber parameters offer valuable guidance for future design and pipeline integrity management of liner systems. These findings are advantageous for this project and also beneficial to the CIPP liner industry.